Measurements of g factors and lifetimes of low-lying states in $^{62-70}$Zn and their shell model implication

O. Kenn,[1] K.-H. Speidel,[1] R. Ernst,[1] S. Schielke,[1] S. Wagner,[1] J. Gerber,[2] P. Maier-Komor,[3] and F. Nowacki[2]
[1]*Institut für Strahlen-und Kernphysik, Universität Bonn, Nußallee 14-16, D-53115 Bonn, Germany*
[2]*Institut de Recherches Subatomique, F-67037 Strasbourg, France*
[3]*Physik-Department, Technische Universität München, James-Franck-Str., D-85748 Garching, Germany*
(Received 2 October 2001; published 14 February 2002)

The g factors of the first 2^+ states and the $B(E2)$ values of the $(2_1^+ \rightarrow 0_1^+)$ transitions have been determined with high precision for all stable doubly even Zn isotopes employing the combined technique of projectile Coulomb excitation in inverse kinematics and transient magnetic fields. In addition, this systematic study was supplemented by a first measurement of radioactive ^{62}Zn ($T_{1/2}=9.2\ h$) formed in an α-transfer reaction with a ^{58}Ni beam. The $g(2_1^+)$ values obtained are in good agreement with previous data but provide considerably higher accuracy. The same quality of agreement was found for the $B(E2)$ values with the exception of ^{70}Zn where the measured value is slightly smaller. The experimental data were compared with large scale shell model calculations considering configurations in the fp and fpg model spaces with inert cores of ^{40}Ca and ^{56}Ni, respectively.

DOI: 10.1103/PhysRevC.65.034308 PACS number(s): 21.10.Ky, 25.70.De, 27.50.+e

I. INTRODUCTION

In the following contribution we report on an investigation of the nuclear structure of Zn isotopes at low excitation energies through measurements of g factors and lifetimes. The present work is an extension of recent experiments on Ni isotopes where the data had been very well explained in the framework of large scale shell model calculations [1,2]. In this particular case it was demonstrated that ^{56}Ni must be abandoned as an inert core. Both the measured $g(2_1^+)$ factors and $B(E2)$ values could only be reproduced by including particle excitations from the $0f_{7/2}$ shell. In fact, a closed ^{40}Ca core and excitations of both protons and neutrons from the $0f_{7/2}$ shell into the remaining fp shell orbits ($1p_{3/2}$, $0f_{5/2}$, and $1p_{1/2}$) were together with a well established effective nucleon-nucleon interaction the essential ingredients of these calculations.

This experience has motivated us to extend the investigations to even heavier nuclei in this mass region. For the Zn isotopes ^{62,64,66,68,70}Zn, with two protons and 4–12 neutrons outside the doubly magic $N=Z=28$ shell, transitions from single particle to collective degrees of freedom are expected. This scenario has been previously discussed in several theoretical papers based on the nuclear shell model as well as particle core coupling calculations [3–6]. With respect to the shell model frame the restriction of the configuration space to the fp orbits must be suspended by including occupations of the $0g_{9/2}$ orbit. In odd-mass isotopes $g_{9/2}$ single particle states are clearly identified at low excitation energies. There is further evidence that particulary for the heavier Zn isotopes the wave functions of low energy states have strong components of this configuration.

Moreover, in a recent study of high spin states in ^{62}Zn superdeformation was found for the first time in this mass region [7]. This phenomenon was expected from calculations predicting large shell gaps in the single particle energies for proton and neutron numbers $N,Z=30$–32 [8,9]. Because of the small number of valence particles in these nuclei and their proximity to the $N=Z$ line nuclear structure studies are of particular interest since reliable microscopic calculations are available to examine the specific influence of isospin symmetry and neutron-proton pairing correlations.

For the low level structure of stable Zn isotopes g factors of the first 2^+ states were determined with relatively low precision in two independent measurements [10,11]. In both experiments the technique of transient magnetic fields was applied. Coulomb excited Zn ions recoiled through thin ferromagnetic iron layers [10] or were stopped in ferromagnetic gadolinium [11]. The measured precessions were relatively small in Fe host due to the short interaction times and the lower field strength compared to Gd, or had to be corrected for static field contributions in the Gd host.

In the present measurements the experimental conditions were considerably improved for all isotopes aiming at substantially higher precision of both g factors and lifetimes of the first excited 2^+ states. This goal was achieved employing the newly developed technique of projectile Coulomb excitation in inverse kinematics combined with transient magnetic fields [12,13]. The method allows us to perform measurements on accelerated and isotopically pure Zn beams using the same multilayered target consisting of a light target layer for Coulomb excitation and a ferromagnetic layer for precession of the nuclear excited state.

Lifetimes of the excited states were measured simultaneously with the g factors employing the Doppler shift attenuation method (DSAM). Deduced $B(E2)$ values are sensitive to the collectivity of the states of interest. It is noted that the magnitude of the g factors is only weakly dependent on the lifetimes of the excited states as long as these are larger than the transit times of the ions through the ferromagnetic target layer.

II. EXPERIMENTAL DETAILS

In the present measurements isotopically pure Zn beams were provided in their natural abundance as ZnO^- by the ion

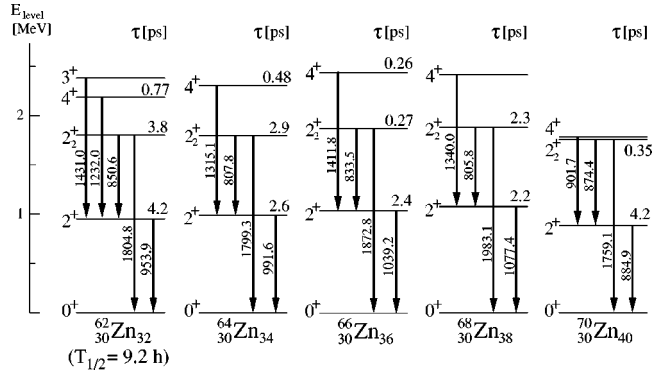

FIG. 1. Low-lying states of $^{62-70}$Zn [21–25].

source of the Munich tandem accelerator and accelerated to energies of 160 MeV with intensities of about 20 nA. For the least abundant ^{70}Zn isotope (0.6%) the beam current on the target was only 2 nA which, however, was sufficient to obtain accurate data due to the high efficiency of the experimental method. The beam ions were Coulomb excited to the first 2^+ state by a natural carbon layer of a multilayered target which had been already used in several earlier experiments (see, e.g., Ref. [1]). It consisted of a 0.45-mg/cm^2 ^{nat}C layer deposited on a 3.82-mg/cm^2 gadolinium layer evaporated at 800 K [14] on a 1-mg/cm^2 tantalum foil followed by a 3.5-mg/cm^2 copper layer. The copper backing served as a hyperfine interaction-free environment for the stopped Zn ions and provided good thermal conductivity to eliminate beam heating effects. The target was cooled to liquid nitrogen temperature and magnetized by an external field of 0.06 T. In default of a radioactive ^{62}Zn beam this nucleus was produced in an α-transfer reaction by bombarding the above-mentioned target with a ^{58}Ni beam of 155 MeV following the reaction ^{12}C(^{58}Ni,2α)^{62}Zn*. In this reaction the first 2^+ state is predominantly populated whereas higher-lying states are only weakly excited. This selectivity has a distinctly different character from that of a fusion evaporation reaction in which states of high energies and spins are populated and the low-lying states are fed via cascade transitions. The absence of strong feeding ensures a clean measurement of the precession of the 2_1^+ state. It is noted that the same strength of α transfer has been observed with Ti and Cr beams using carbon as target [15,16]. Such a reaction has recently been used to measure the g factor of the first 2^+ state of ^{54}Cr [16].

The γ rays emitted from the excited 2^+ states of the different isotopes (see Fig. 1) were measured in coincidence with forward scattered carbon ions or the 2 α particles (from the decay of ^{8}Be in the α-transfer reaction) using 9×9-cm BaF_2 scintillators. A Ge detector of 23% relative efficiency was placed at 0° to the beam direction and served as monitor for contaminant lines and for the measurement of nuclear lifetimes via the DSAM technique. Like in several former experiments with other ion beams and using the same target, fusion reactions with carbon nuclei (associated with light particle emission) contributed a negligible background in the γ-coincidence spectra, showing that carbon is ideally suited for this type of spectroscopic studies. Figure 2 shows typical γ spectra from Coulomb excitation of 160-MeV ^{64}Zn projectiles. In contrast to ^{58}Ni beams α-transfer reactions with Zn beams of 160 MeV leading to Ge isotopes are obviously suppressed. The reason is that the reaction with a ^{58}Ni beam takes place close to the Coulomb barrier whereas the ^{64}Zn beam energy is appreciably lower ($\simeq$20 MeV). This different behavior is clearly seen in the coincidence particle spectra [Fig. 3(a)] where the low energy α peak is well pronounced with a ^{58}Ni beam but completely absent with a ^{64}Zn beam. These spectra were obtained by detecting the forward scattered ions in a Si detector with nominal thickness of 100 μm placed at 0° and subtending an angle of $\pm20°$. For this geometry the beam had to be stopped in a tantalum foil (placed behind the target) whose thickness allowed the carbon ions and α particles to pass through to the Si detector. For the clean separation of α's from the carbon ions due to

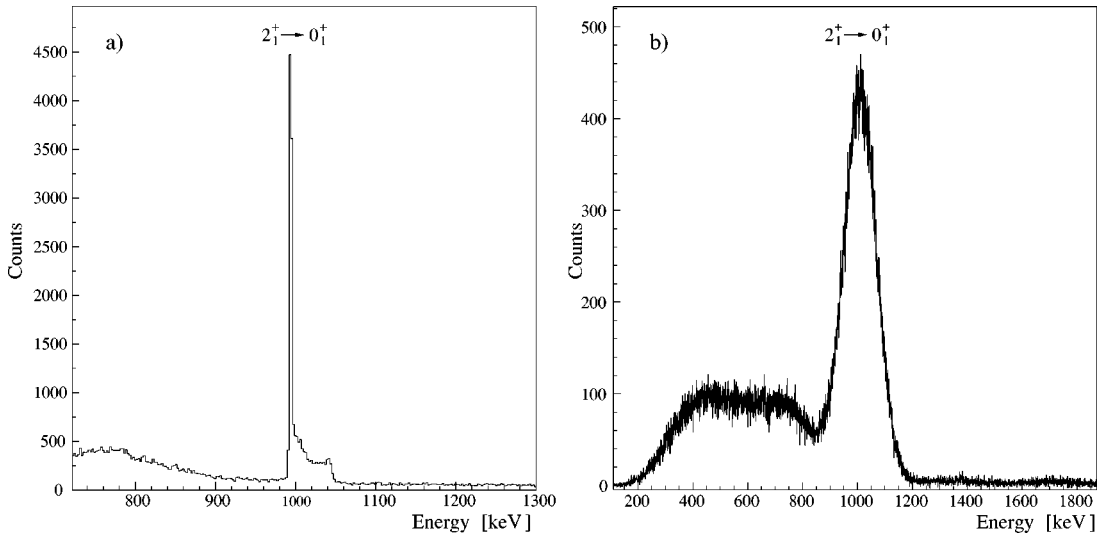

FIG. 2. ^{64}Zn γ-ray spectra observed with (a) Ge detector and (b) BaF_2 scintillator in coincidence with carbon ions of the particle spectrum [see Fig. 3(b)].

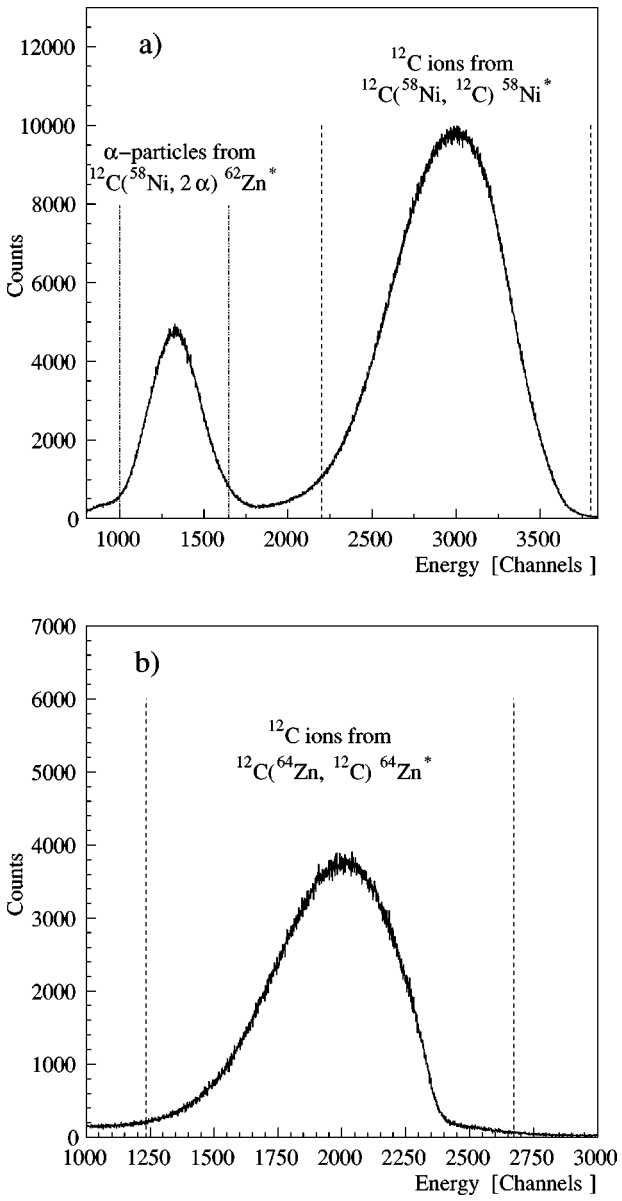

FIG. 3. Particle spectra obtained with a 100-μm Si detector at low bias in coincidence with all γ rays for (a) ^{58}Ni and (b) ^{64}Zn beams. The α particles in (a) associated with ^{62}Zn are well separated from the carbon ions corresponding to Coulomb excited ^{58}Ni.

incomplete stopping of the light particles in a reduced depletion layer the Si detector was operated at a very low bias ($\simeq$5 V). By gating either on the carbon ions or the α peak (see Fig. 3), only γ lines from Coulomb excitation of the beam ions or nuclei following α transfer appear in the spectra (Fig. 4). Hence the poor energy resolution of the scintillators was no impediment to obtaining a clean spectroscopy. As evident from Fig. 4 the ^{62}Zn spectrum has a rather simple structure in which the most prominent γ line refers to the $(2_1^+ \rightarrow 0_1^+)$ transition whereas the higher excited states are only weakly populated.

Particle-γ-angular correlations $W(\Theta_\gamma)$ and anisotropies $W(\theta_\gamma=50°)/W(\theta_\gamma=80°)$ have been measured for the $(2_1^+ \rightarrow 0_1^+)$ transition of each isotope in order to determine the

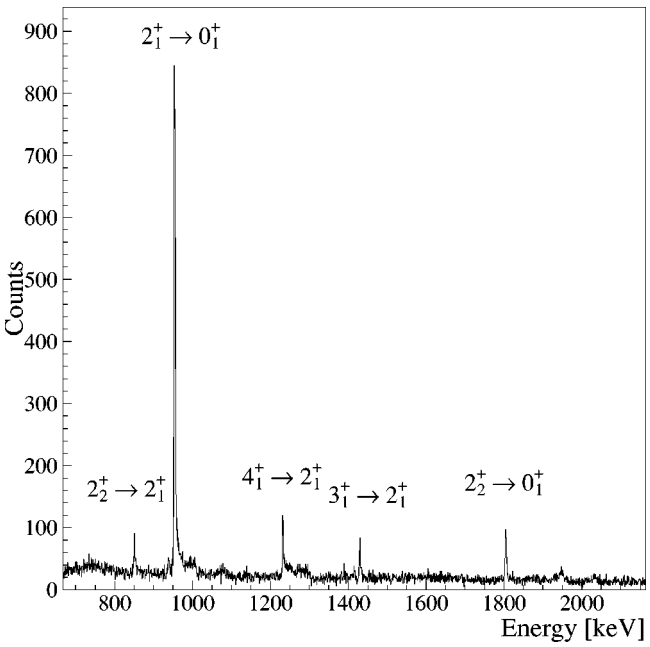

FIG. 4. γ rays observed with the Ge detector in coincidence with the α-particle peak in the particle spectrum [Fig. 3(a)]. All γ-ray lines identified belong to the de-excitation of ^{62}Zn states populated in the α-transfer reaction.

logarithmic slopes, $S=[1/W(\theta_\gamma)][dW(\theta_\gamma)/d\theta_\gamma]$ in the rest frame of the emitting nuclei at the angle $\theta_\gamma=65°$ where the sensitivity to the precessions was optimal. Whereas the spin alignment was rather good for Coulomb excitation only small anisotropies were found in the α-transfer reaction. In case of ^{62}Zn$(2_1^+ \rightarrow 0_1^+)$ the slope value was derived from a detailed measurement of the angular correlation between α particles and γ's (Fig. 5). A slightly larger anisotropy was obtained by inserting a vertical slit mask in front of the Si detector. The measured slopes are summarized in Table I.

Precession angles Φ^{exp} were derived from double ratios $DR(i/j)=(N_i\uparrow/N_i\downarrow)/(N_j\uparrow/N_j\downarrow)$ of coincident counting rates N with an external field applied perpendicular to the γ-detection plane, alternately in the ''up'' and ''down'' directions. The indices i,j represent a pair of γ detectors symmetric to the beam axis. The precession angles are given by

$$\Phi^{exp}=\frac{1}{S}\cdot\frac{\sqrt{DR}-1}{\sqrt{DR}+1}=g\cdot\frac{\mu_N}{\hbar}\int_{t_{in}}^{t_{out}}B_{TF}[v_{ion}(t)]\cdot e^{-t/\tau}dt, \tag{2.1}$$

where g is the g factor of the 2_1^+ state and B_{TF} is the transient field acting on the nucleus during the time interval $(t_{out}-t_{in})$ which the ions spend in the gadolinium layer; the exponential accounts for nuclear decay with lifetime τ.

The lifetimes of the first 2^+ states of all Zn isotopes and the 4^+ state of ^{62}Zn have been determined in DSAM measurements. The high velocities (Table I) implied high sensitivity for the lifetimes in the picosecond range. The Doppler broadened shapes of the γ-ray lines were fitted for the reaction kinematics applying stopping powers [17] to Monte Carlo simulations and including the second order Doppler

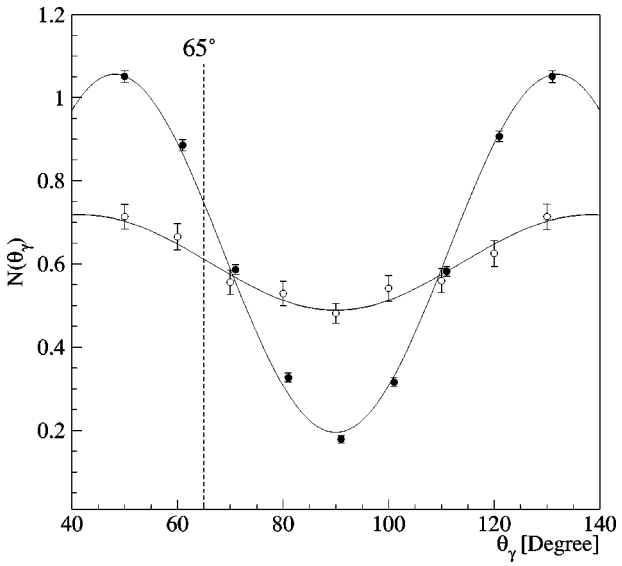

FIG. 5. Measured γ-angular correlations for the ^{58}Ni($2_1^+ \rightarrow 0_1^+$) transition (solid points) and the ^{62}Zn($2_1^+ \rightarrow 0_1^+$) transition (open points) with least squares fits to the data. The dashed line at $\Theta_\gamma = 65°$ refers to the detector position for the precession measurements (see text).

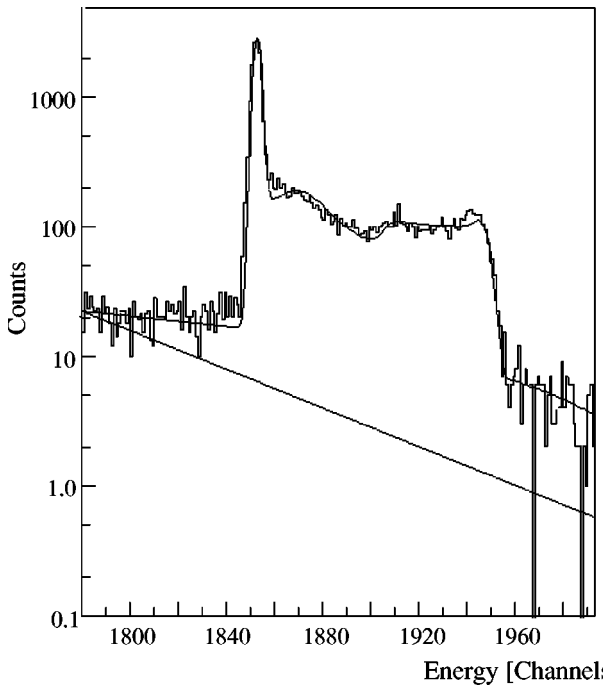

FIG. 6. DSAM fit to the Doppler broadened shape of the ^{66}Zn($2_1^+ \rightarrow 0_1^+$) γ line including a linear background.

effect as well as the finite size and the energy resolution of the Ge detector. Feeding from higher states could be neglected. The computer code LINESHAPE [18] was used in the analysis. The high quality of a typical line-shape fit achieved is shown in Fig. 6. It is noted that characteristic structures of the line shape from the slowing down of the ions in the different target layers are very well reproduced. The measured lifetimes are summarized in Table II together with values quoted in the literature.

III. RESULTS AND INTERPRETATION

The *g* factors were derived from the experimental precession angles by determining the effective transient field B_{TF} on the basis of the empirical linear parametrization (see, e.g., Ref. [15]):

$$B_{TF}(v_{ion}) = G_{beam} \cdot B_{lin} \tag{3.1}$$

with

$$B_{lin} = a(Gd) \cdot Z_{ion} \cdot \frac{v_{ion}}{v_0}, \tag{3.2}$$

where the strength parameter $a(Gd) = 17(1)$ T [15], $v_0 = e^2/\hbar$, and $G_{beam} = 0.64(6)$ is the attenuation factor accounting for the demagnetization of the gadolinium layer induced by the ion beam [19]. This value is close to that used for the experiments with Ni beams [$G_{beam} = 0.69(6)$ [2]] on the same target accounting for small differences in the conditions of present Zn ions. For ^{62}Zn involving ^{58}Ni beams the attenuation factor is identical to that used for the Ni experiments [2]. Beyond that, many other experimental data

TABLE I. Summary of the average velocities of the ions entering, exiting, and traversing the ferromagnetic Gd foil, the measured logarithmic slopes of the angular correlations at $|\theta_\gamma| = 65°$, and the precession angles Φ^{exp}. The Φ^{lin}/g values were calculated using Eqs. (2.1), (3.1), and (3.2).

Nucleus	$E_x(2_1^+)$ [MeV]	$\langle v/v_0 \rangle_{in}$	$\langle v/v_0 \rangle_{out}$	$\langle v_{ion}/v_0 \rangle$	$\lvert S(65°) \rvert$	Φ^{exp} [mrad]	$\frac{\Phi^{lin}}{g}$ [mrad]
^{62}Zn	0.954	7.9	4.8	6.3	0.408(51)[a]	14.63(6.26)	35.5(3.1)
		7.7	4.5	6.0	0.591(73)[b]	12.55(3.91)	35.4(3.1)
^{64}Zn	0.992	6.5	3.5	4.9	2.139(23)	13.92(62)	31.3(2.9)
^{66}Zn	1.039	6.5	3.5	4.9	2.113(38)	12.38(54)	31.0(2.9)
^{68}Zn	1.077	6.5	3.6	5.0	2.151(38)	13.38(71)	30.7(2.9)
^{70}Zn	0.885	6.4	3.6	4.9	2.471(38)	12.51(77)	33.1(3.1)

[a]Beam energy 160 MeV.
[b]Beam energy 155 MeV.

TABLE II. Comparison of the measured g factors and lifetimes with data from literature.

Nucl.(I^π)	τ [ps]		$g(2_1^+)$		
	Refs. [21–25]	Present	Ref. [10]	Ref. [11]	Present
^{62}Zn(2_1^+)	4.2(3)	4.3(3)			+0.371(99)
(4_1^+)	0.76($^{+34}_{-20}$)	1.2(1)			
^{64}Zn(2_1^+)	2.60(6)	2.70(8)	+0.42(8)	+0.46(10)	+0.445(46)
^{66}Zn(2_1^+)	2.38(9)	2.43(5)	+0.26(7)	+0.47(11)	+0.399(41)
^{68}Zn(2_1^+)	2.18(9)	2.32(7)	+0.50(9)	+0.46(14)	+0.436(47)
^{70}Zn(2_1^+)	4.2(4)	5.3(3)	+0.30(7)	+0.30(7)	+0.378(42)

were included which describe the dependence of the attenuation on parameters such as the stopping power and intensity of the beam ions in ferromagnetic gadolinium as well as on the electron orbitals of the projectile ions relevant for the transient field strength [19,20] (see also discussion in Ref. [2]).

The experimental precession angles are summarized in Table I. For the ^{62}Zn result several runs were needed to obtain sufficient accuracy of the g factor. The reason lies in the small slope value of the angular correlation and the thus reduced sensitivity to the precession. The precessions Φ^{lin}/g listed in the table were calculated using Eqs. (2.1), (3.1), and (3.2). Table II summarizes the measured g factors and lifetimes. These have been compared with adopted values quoted in the literature [21–25]. With the exception of ^{70}Zn(2_1^+) all lifetimes were very well confirmed with an accuracy sometimes better than that of the adopted value which is an average of several independent measurements. In case of ^{70}Zn the measured lifetime is found to be significantly larger. For ^{62}Zn a lifetime was obtained also for the 4^+ state with much higher precision than that quoted in the literature. For all isotopes the new g factor values agree very well with earlier data.

The new data of g factors and $B(E2)$'s of the present work were compared with results from large scale shell model calculations (LSSM) assuming two different configuration spaces (Table III): model space I (LSSM I) [26,27] refers to an inert ^{40}Ca core and including the $0f_{7/2}$, $1p_{3/2}$, $1p_{1/2}$, and $0f_{5/2}$ valence orbitals. Due to the extremely large dimensionalities involved, the configuration space was restricted to a maximum of four particle–four hole excitations for ^{62}Zn and ^{64}Zn. This restriction, however, has only a minor influence on the calculated quantities. For example in ^{66}Zn, the energy gain between the $4p4h$ space and the full space results is only 17 keV. The effective interaction used for the calculations is KB3G from Ref. [28].

Model space II (LSSM II) is based on a ^{56}Ni core and including the $0f_{5/2}$, $1p_{3/2}$, $1p_{1/2}$, and $0g_{9/2}$ valence orbitals. The two-body matrix elements are from a G matrix calculation [29,30] whose monopoles have been modified to reproduce energy systematics in Ni isotopes and $N=50$ isotones [26,27].

All calculations were performed with the computer code ANTOINE [31]. A polarization effective charge of 0.5 was used for $E2$ rates and effective g factors $g^s_{eff}=0.75g^s_{free}$ and $g^l(\pi)=1.1$, $g^l(\nu)=-0.1$ for the magnetic moments.

In view of the results and discussions from our previous work on Ni isotopes [1,2], the fp valence space is expected to be relevant up to neutron number $N=36$, but the inclusion of the $g_{9/2}$ orbital becomes extremely important for describing the heavier Zn isotopes. This feature was also emphasized in earlier calculations (see, e.g., Ref. [3]).

The new g factor data are displayed in Fig. 7 together with the results of LSSM (I+II) calculations (see also Table III). As expected, the LSSM I results are in rather good

TABLE III. Comparison of present experimental g factors and B(E2) values in Weisskopf units with results from large-scale shell model calculations LSSM I and LSSM II (see text).

Nucl. (I^π)	$B(E2)$ [W.u.]			$g(I^\pi)$		
	Expt.	LSSM I	LSSM II	Expt.	LSSM I	LSSM II
^{62}Zn(2_1^+)	17(1)	16.9	11.4	+0.371(99)	+0.46	+0.467
(4_1^+)	16(1)	19.8	15.0		+0.57	+0.448
^{64}Zn(2_1^+)	20.7(6)	15.4	11.3	+0.445(46)	+0.48	+0.448
(4_1^+)		15.3	14.3		+0.73	+0.362
^{66}Zn(2_1^+)	17.5(4)	12.5	10.5	+0.399(41)	+0.48	+0.578
(4_1^+)		13.8	12.9		+0.74	+0.436
^{68}Zn(2_1^+)	14.7(4)	9.0	9.7	+0.436(47)	+0.58	+0.733
(4_1^+)		3.3	10.9		+1.08	+0.404
^{70}Zn(2_1^+)	16.5(9)	4.4	9.7	+0.378(42)	+1.70	+0.633
(4_1^+)		1.1	11.1		+1.22	+0.357

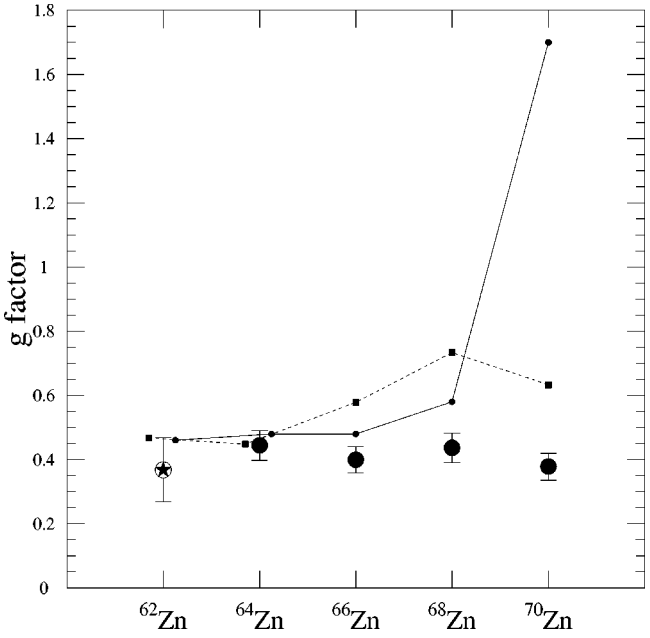

FIG. 7. Experimental g factors of 2_1^+ states (large solid points and star) are compared with results from shell model calculations. Small circles refer to a ^{40}Ca core (LSSM I), and squares to a ^{56}Ni core (LSSM II). The lines are drawn to guide the eye (see text).

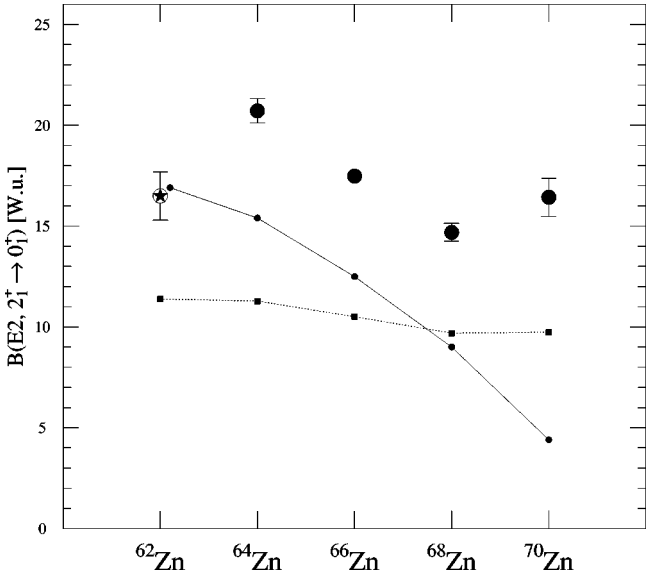

FIG. 8. Experimental $B(E2)$'s of $(2_1^+ \rightarrow 0_1^+)$ in Weisskopf units (large solid points and star) are compared with results from shell model calculations. Small circles refer to a ^{40}Ca core (LSSM I), and squares to a ^{56}Ni core (LSSM II). The lines are drawn to guide the eye (see text).

agreement with the values for ^{62}Zn to ^{66}Zn. As for the experimental data, the calculations show almost no dependence on the neutron number for these isotopes. The rise (not seen in the experimental data) for ^{68}Zn and ^{70}Zn simply reflects subshell closures in the limited fp valence space. The striking deviation from the experimental data is therefore a strong indication for a larger valence space including the $0g_{9/2}$ orbital. The importance of the $0g_{9/2}$ orbital for describing the heavy Zn isotopes originates from the strong $T=1$ attraction between the $0f_{5/2}$, $1p_{3/2}$, $1p_{1/2}$, and the $0g_{9/2}$ orbitals: at the end of the fp shell, filling the neutrons brings down the $0g_{9/2}$ shell. Its spectacular effect on the g factor of ^{70}Zn is shown by the LSSM II result which explicity includes this orbital. Evidently, for the other isotopes, the excitation of particles from the $0f_{7/2}$ shell improves the agreement with the data (see Table III and Fig. 7). The same tendency was seen in the calculations for the Ni isotopes smoothing the g factor dependence on neutron number [1,2]. On the other hand, the vanishingly small difference between the LSSM I and II results for the g factors of ^{62}Zn and ^{64}Zn shows that the excitation of particles from the $0f_{7/2}$ shell and the population of the $0g_{9/2}$ orbital play only a minor role for the light Zn nuclei (see Fig. 7). This feature, however, is not seen in the $B(E2)$ values (see below).

In view of these results large scale shell model calculations in the fpg valence space, beyond a ^{40}Ca core, would certainly be optimum which, however, are at present not feasible due to computer limitations. An almost equivalent approach in this direction are calculations considering a ^{48}Ca core, with $0f_{7/2}$, $1p_{3/2}$, $1p_{1/2}$, and $0f_{5/2}$ active proton orbitals and $0f_{5/2}$, $1p_{3/2}$, $1p_{1/2}$, and $0g_{9/2}$ active neutron orbitals. A preliminary result for ^{70}Zn in this valence space yields for the g factor $g(2_1^+)=+0.45$ [32] which is indeed close to the experimental value.

Similar behavior is found for the $B(E2)$ values (see Fig. 8). LSSM I calculations reproduce rather well the trend of the experimental data of $^{62-68}$Zn while the LSSM II calculations undervalue the data due to the $N=Z=28$ shell closure. The LSSM I results yield slightly weaker transition rates; the reason is not clear and could originate from fluctuations of the effective charge or lack of the quadrupole strength for the $0f_{5/2}$, $1p_{3/2}$, $1p_{1/2}$ matrix elements. For ^{70}Zn again, the exclusion of the $0g_{9/2}$ neutron orbital has a strong effect. Like for the g factor, again a dramatic change is obtained by including this orbital to a ^{48}Ca core. The calculations in this valence space yield for ^{70}Zn $B(E2,2_1^+ \rightarrow 0_1^+)=15.4$ Weisskopf units in excellent agreement with the experimental value of 16.5(9) W.u. Another interesting result is that the rather accurate $B(E2)$ value of the $(4_1^+ \rightarrow 2_1^+)$ transition in ^{62}Zn agrees very well with both LSSM I and II calculations (Fig. 9 and Table III). More accurate measurements for the heavier isotopes are highly desirable to test the calculations which predict a decrease of the $B(E2;4_1^+ \rightarrow 2_1^+)$'s with increasing neutron number in contrast to previous data.

IV. SUMMARY AND CONCLUSIONS

Summarizing the present work, it has been shown that projectile Coulomb excitation in inverse kinematics is a powerful technique in combination with transient magnetic fields for g factor measurements of series of isotopes. It requires advanced ion source techniques in accelerators to provide the various isotopes as beams with high efficiency. This potential was effectively exploited for the Zn experiments

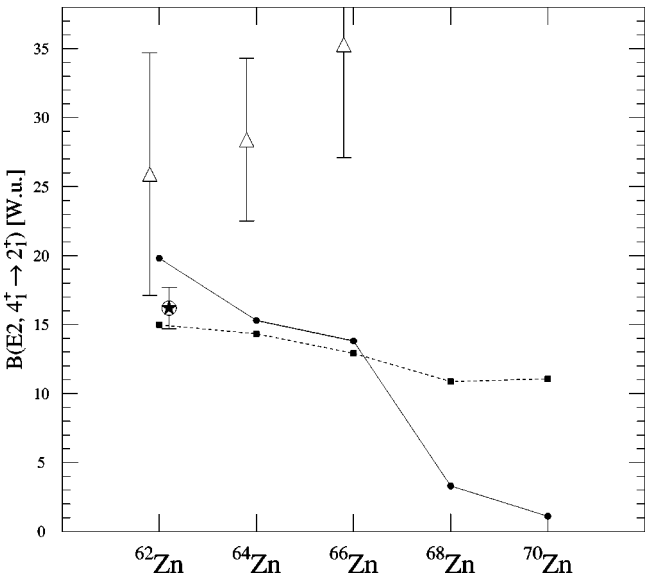

FIG. 9. Experimental $B(E2)$'s of $(4_1^+ \rightarrow 2_1^+)$ in Weisskopf units are compared with results from shell model calculations. The value marked by a star refers to the present measurements whereas the other data (triangles) are taken from Refs. [21–25]. Small circles refer to a ^{40}Ca core (LSSM I), and squares to a ^{56}Ni core (LSSM II). The lines are drawn to guide the eye (see text).

where the natural isotopic abundances were sufficient to provide the necessary beam intensities of the isotopically separated ions on the target. It is the kinematic focussing of both the beam ions and the target nuclei in the nuclear reaction which makes these measurements so efficient even with low intensity beams. The biggest challenge in the present studies were the measurements with beams of ^{70}Zn with its natural abundance of only 0.6%.

The other important result of the present investigations is the use of α transfer to beam ions for populating selective states of unstable nuclei. Although the spin alignment of the excited states is poor and therefore the anisotropy of the γ-angular correlation small, it still enables to measure g factors of radioactive nuclei. This is shown by the successful measurements on current ^{62}Zn and former ^{54}Cr [16].

The present results on g factors and $B(E2)$'s strongly request a large configuration space in the shell model calculations including the $0f_{7/2}$ shell below ^{56}Ni and the $g_{9/2}$ intruder orbit in addition. That ^{40}Ca is a more suitable core than ^{56}Ni was also an essential feature for explaining the Ni data [1,2]. In view of the new and very encouraging results for ^{70}Zn a ^{48}Ca core seems to be a highly valuable compromise for describing the Zn nuclei. This finding reflects the well-known fact that the neutron $N=28$ shell closure is a rather stable configuration. Moreover, the calculated g factors of 4^+ states imply large variations compared to the 2^+ values which should certainly be investigated by similar measurements. These require, however, higher beam energies to enhance the Coulomb excitation cross sections.

Finally, there is no clear evidence for the $f_{5/2}$ subshell closure at ^{68}Zn by the present data although the $B(E2)$ value of ^{68}Zn tends to be slightly smaller compared to neighboring isotopes.

ACKNOWLEDGMENTS

The authors are grateful to the operators of the Munich tandem accelerator for their extraordinary cooperation in providing optimum beam conditions during the experiment. Support by the BMBF and the Deutsche Forschungsgemeinschaft is acknowledged.

[1] O. Kenn, K.-H. Speidel, R. Ernst, J. Gerber, N. Benczer-Koller, G. Kumbartzki, P. Maier-Komor, and F. Nowacki, Phys. Rev. C **63**, 021302(R) (2001).
[2] O. Kenn, K.-H. Speidel, R. Ernst, J. Gerber, P. Maier-Komor, and F. Nowacki, Phys. Rev. C **63**, 064306 (2001).
[3] J.F.A. van Hienen, W. Chung, and B.H. Wildenthal, Nucl. Phys. **A269**, 159 (1976).
[4] V. Lopac and V. Paar, Nucl. Phys. **A297**, 471 (1978).
[5] H.F. De Vries and P.J. Brussard, Z. Phys. A **286**, 1 (1978).
[6] Y. Sun, Jing-ye Zhang, M. Guidry, J. Meng, and S. Im, Phys. Rev. C **62**, 021601(R) (2000).
[7] C.E. Svensson, C. Baktash, J.A. Cameron, M. Devlin, J. Eberth, S. Flibotte, D.S. Haslip, D.R. LaFosse, I.Y. Lee, A.O. Macchiavelli, R.W. McLeod, J.M. Nieminen, S.D. Paul, L.L. Riedinger, D. Rudolph, D.G. Sarantites, H.G. Thomas, J.C. Waddington, W. Weintraub, J.N. Wilson, A.V. Afansjev, and I. Ragnarsson, Phys. Rev. Lett. **79**, 1233 (1997).
[8] R.K. Sheline, I. Ragnarsson, and S.G. Nilsson, Phys. Lett. **41B**, 115 (1972).
[9] J. Dudek, W. Nazarewicz, Z. Szymanski, and G.A. Leander, Phys. Rev. Lett. **59**, 1405 (1987).
[10] N. Benczer-Koller, M. Hass, T.M. Brennan, and H.T. King, J. Phys. Soc. Jpn. **44**, 341 (1978).
[11] C. Fahlander, K. Johansson, and G. Possnert, Z. Phys. A **291**, 93 (1979).
[12] K.-H. Speidel, N. Benczer-Koller, G. Kumbartzki, C. Barton, A. Gelberg, J. Holden, G. Jakob, N. Matt, R.H. Mayer, M. Satteson, R. Tanczyn, and L. Weissman, Phys. Rev. C **57**, 2181 (1998).
[13] R. Ernst, K.-H. Speidel, O. Kenn, U. Nachum, J. Gerber, P. Maier-Komor, N. Benczer-Koller, G. Jakob, G. Kumbartzki, L. Zamick, and F. Nowacki, Phys. Rev. Lett. **84**, 416 (2000).
[14] P. Maier-Komor, K.-H. Speidel, and A. Stolarz, Nucl. Instrum. Methods Phys. Res. A **334**, 191 (1993).
[15] R. Ernst, K.-H. Speidel, O. Kenn, A. Gohla, U. Nachum, J. Gerber, P. Maier-Komor, N. Benczer-Koller, G. Kumbartzki, G. Jakob, L. Zamick, and F. Nowacki, Phys. Rev. C **62**, 024305 (2000).
[16] S. Wagner, K.-H. Speidel, O. Kenn, R. Ernst, S. Schielke, J. Gerber, P. Maier-Komor, N. Benczer-Koller, G. Kumbartzki, Y.Y. Sharon, and F. Nowacki, Phys. Rev. C **64**, 034320 (2001).

[17] F.J. Ziegler, J. Biersack, and U. Littmark, *The Stopping and Range of Ions in Solids* (Pergamon, Oxford, 1985), Vol. 1.
[18] J.C. Wells and N.R. Johnson, program LINESHAPE, 1994, ORNL.
[19] G. Jakob, J. Cub, K.-H. Speidel, S. Kremeyer, H. Busch, U. Grabowy, A. Gohla, O. Jessensky, and J. Gerber, Z. Phys. D: At., Mol. Clusters **32**, 7 (1994).
[20] K.-H. Speidel, U. Reuter, J. Cub, W. Karle, F. Passek, H. Busch, S. Kremeyer, and J. Gerber, Z. Phys. D: At., Mol. Clusters **22**, 371 (1991).
[21] Huo Junde and B. Singh, Nucl. Data Sheets **91**, 395 (2000).
[22] B. Singh, Nucl. Data Sheets **78**, 462 (1996).
[23] M.R. Bath, Nucl. Data Sheets **83**, 832 (1998).
[24] M.R. Bath, Nucl. Data Sheets **76**, 349 (1995).
[25] M.R. Bath, Nucl. Data Sheets **68**, 124 (1993).
[26] F. Nowacki, Ph.D. thesis, IReS, Strasbourg, 1996.
[27] E. Caurier, F. Nowacki, A. Poves, and J. Retamosa, Phys. Rev. Lett. **77**, 1954 (1996).
[28] A. Poves, J. Sanchez-Solano, E. Caurier, and F. Nowacki, Nucl. Phys. **A694**, 157 (2001).
[29] M. Hjorth-Jensen (private communication).
[30] M. Hjorth-Jensen, T.T.S. Kuo, and E. Osnes, Phys. Rep. **261**, 125 (1995).
[31] E. Caurier, computer code ANTOINE, Strasbourg, 1989.
[32] A. Poves, Eur. Phys. J. (to be published).